On the recent seismic activity in North-Eastern Aegean Sea including the M_w5.8 earthquake on 8 January 2013

By Nicholas V. Sarlis[*1,†]

(Communicated by Seiya Uyeda, M.J.A.)

Abstract: In the last week of November 2012, we announced that a strong electrotelluric disturbance, which we judged to be a Seismic Electric Signal (SES) activity, was recorded at station Assiros located in Northern Greece. This disturbance was actually followed by an M_w5.8 earthquake on 8 January 2013 in North-Eastern Aegean Sea. Here we show that, by analyzing this SES activity and employing the natural time analysis of subsequent seismicity, we estimated the epicentral location, magnitude and occurrence time which are reasonably compatible with those of the M_w5.8 event.

Keywords: Seismic Electric Signals, natural time, epicentral location, earthquake magnitude, time-window

1. Introduction

Recent studies[1)–3)] have strengthened the importance of general seismo-electromagnetics in earthquake (EQ hereafter) prediction. There have been suggested[1)–3)] various promising candidates for EQ prediction, the measurement[4)–7)] of Seismic Electric Signals is one of them for which their correlation with EQs has been intensively studied[4)–13)] with positive results, *e.g.* for a recent review see Ref. 14. In this paper, we intend to report on the possible relationship between the Seismic Electric Signals observed at Assiros station in Northern Greece on 13 July 2012 (see Fig. 1) and an M_w5.8 EQ which occurred on 8 January 2013 in North-Eastern Aegean Sea. We shall show that the epicenter, magnitude and occurrence time of the impending EQ estimated before its occurrence conform to those of the actual EQ.

Continuous measurements of the electric field of the Earth in Greece[4)–9)] (see Fig. 2) and Japan[1),10)–12)] revealed that transient variations of the electric field of the Earth, called Seismic Electric Signals (SES), precede major EQs. When several SESs occur within a short time like a few hours or so, they are called[6)] SES activity. The lead time of SES activity varies between a few weeks and five months or so.[13)] The current configuration of the telemetric network comprising 9 field stations, in each of which a multitude of measuring short and long electric dipoles of length (L) has been installed, can be seen in Fig. 2. The discrimination of SES from noise is based on the four criteria suggested in Ref. 6. Briefly, an electric disturbance is classified as SES if: (a) it is not recorded simultaneously at all stations, (b) at a station, it exhibits an almost constant value of $\Delta V/L$, where ΔV is the potential difference observed for almost parallel short measuring dipoles, (c) it appears simultaneously in both short and long dipoles, and (d) the ΔV values of long and short dipoles are compatible. A sensitive station can record SES only from some specific seismic areas (selectivity effect). A map showing the seismic areas that emit SES detectable at a given station is called[6),7)] selectivity map of this station. For example, the three grey shaded areas of Fig. 2 are the selectivity map of Assiros station (ASS) which was known to us before 8 January 2013 (the day of the M_w5.8 EQ). The above physical properties of SES have been theoretically explained[15),16)] — for a recent review see Ref. 13.

The magnitude of the expected EQ can be estimated by the relation:[5),12)]

$$\log_{10}(E \times r) = aM + b, \qquad [1]$$

[*1] Solid State Section and Solid Earth Physics Institute, Physics Department, University of Athens, Greece.

[†] Correspondence should be addressed: N. V. Sarlis, Solid State Section and Solid Earth Physics Institute, Physics Department, University of Athens, Panepistimiopolis Zografos 15784, Greece (e-mail: nsarlis@phys.uoa.gr).

doi: 10.2183/pjab.89.438

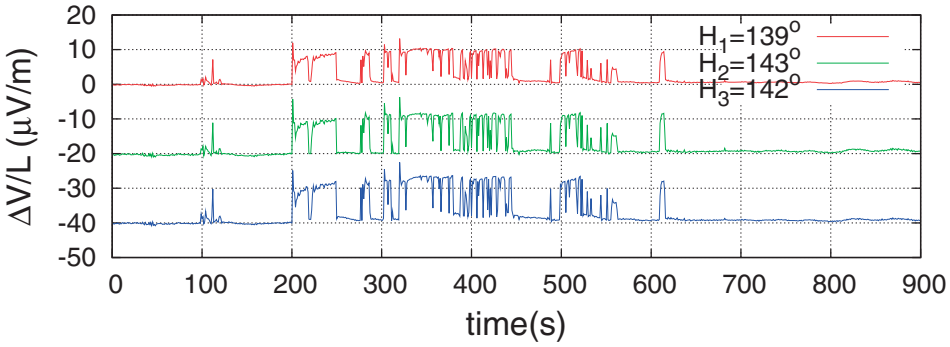

Fig. 1. Recordings of the SES activity at Assiros station at 13 July 2012 at the three — out of sixteen — independent dipoles of different lengths (varying between 500 to 900 m) with true headings H_1, H_2 and H_3 as shown in the legend.

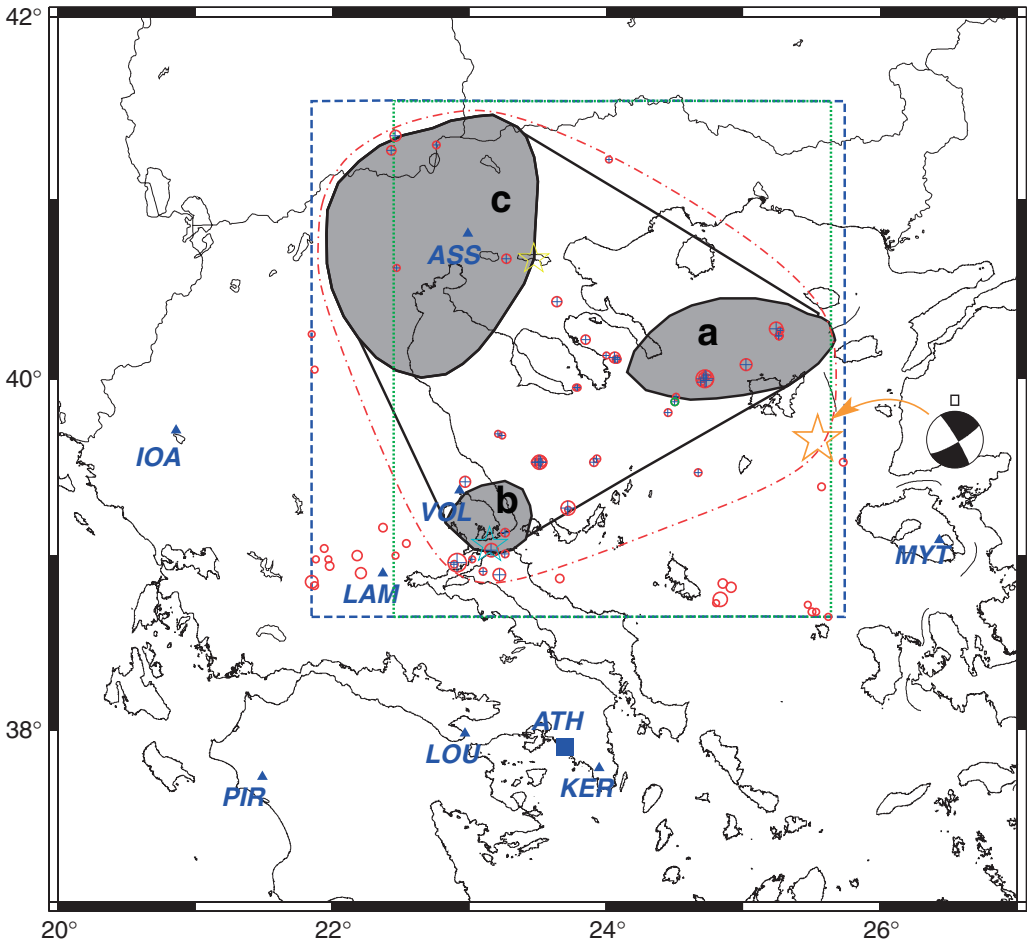

Fig. 2. Map showing the operating field stations (blue triangles) and the central station (blue square). The selectivity map of ASS is also shown: the three areas 'a', 'b', and 'c' may be joined[13] to a single larger area as indicated by a thick solid black curve. The EQs that occurred after the initiation of the SES activity at ASS until 6 January 2013 within the area $N_{38.7}^{41.5}E_{21.9}^{25.7}$ (blue broken rectangle) are depicted by red circles. The area A $N_{38.7}^{41.5}E_{22.5}^{25.6}$ originally used for the estimation of the occurrence time-window of the forthcoming EQ is shown by the green rectangle bounded with dotted lines. The orange star shows the epicenter of the M_w5.8 EQ that occurred on 8 January 2013 whereas its mechanism (USGS Body-Wave Moment Tensor Solution) is the depicted by the beachball. The proposed selectivity map of ASS is bounded with the red dashed-dotted line while the EQs that lie inside it are marked with the blue plus symbols. The cyan and the yellow stars show the epicenters of the M_w5.6 EQ on 30 April 1985 and the M_w5.3 EQ on 4 May 1995, respectively, also discussed in the text.

Table 1. The occurrence date, location and magnitude of the two mainshocks in the areas 'a' and 'b' discussed in the text along with the parameters (SES initiation date, SES amplitude E and focal distance r) of their preceding SES recorded at ASS

SES date	E (μV/m)	r (km)	EQ date	EQ location	M_w
13 July 2012[a]	15	250	8 January 2013	39.66°N,25.54°E	5.8
25 April 1985[b]	14	195	30 April 1985	39.06°N,23.15°E	5.6

[a]See the lowest panel of Fig. 1(b) of Ref. 24.
[b]See Fig. 4 of Ref. 6.

where $E\,(=\Delta V/L)$ is the amplitude of the SES, r is the focal distance from the station, b a station dependent constant, and a a constant lying in the range 0.32–0.37 related with the fractal properties of the SES emitting source, *e.g.* see Ref. 17.

2. Natural time analysis. Background

The analysis of SES was significantly advanced in the new time-domain, termed natural time domain.[13),18)] The real time collection of SESs and their analysis allow announcement of prediction well before the EQ occurrence.

In a time series consisting of N events, the *natural time* $\chi_k = k/N$ serves as an index[18)] for the occurrence of the k-th event. In natural time analysis[13)] the evolution of the pair (χ_k, Q_k) is studied, where Q_k denotes a quantity proportional to the energy released in the k-th event. In the case of seismicity,[13),19)] Q_k is given by

$$Q_k \propto 10^{1.5M} \qquad [2]$$

where M stands for the moment magnitude.

It was shown[13),20)] that when the system enters the critical stage, the variance

$$\kappa_1 \equiv \sum_{k=1}^{N} \chi_k^2 p_k - \left(\sum_{k=1}^{N} \chi_k p_k \right)^2 \qquad [3]$$

of natural time χ weighted by $p_k \equiv Q_k / \sum_{n=1}^{N} Q_n$ approaches the value

$$\kappa_1 = 0.070. \qquad [4]$$

The experiences showed[13),19),21)] that when analyzing the small EQs that occurred after the SES activity initiation in natural time the main shock occurs within a week or so after Eq. [4] is realized, thereby making the time window of prediction appreciably narrower.

3. Comparison of the actual EQ epicenter and magnitude with those estimated from the SES

Figure 2 shows the selectivity map of ASS (grey shaded areas 'a', 'b' and 'c') available to us before the date of the 8 January 2013 M_w5.8 EQ which is also shown by an orange star. The beachball depicts the EQ mechanism by the United States Geological Survey (USGS). Based on this selectivity map, we expected the epicenter of the coming EQ may be in one of the areas 'a', 'b' and 'c'. We observe that the actual EQ epicenter lies about 40 km southeast of area labeled 'a'. This may be regarded as reasonably conforming the prediction.

Moreover, we exclude the area 'c' from the candidate area by the recordings of the long and the short dipoles operating at ASS (for geographic distribution of dipoles, see Figs. 1.1.4, 1.4.1 and 4.2.3 of Ref. 22) as follows. By considering the value of the ratio E_{EW}/E_{NS} of the two SES components (as measured by the short dipoles along the directions EW and NS), we could select the regions from the selectivity map which might have emitted the observed SES. Detailed studies[23)] (see also p. 15 of Ref. 22) have shown that a sensisitve measure of E_{EW}/E_{NS} is the ratio $\Delta V_{long}/\Delta V_{short}$ where ΔV_{long} and ΔV_{short} stand for the ΔV values of the SES measured on a long and a short dipole, respectively (*cf.* this ratio, which is termed "directional parameter" in Ref. 23, was found to change from one epicentral region to another). In particular, in the case of ASS a long dipole ∼10 km long is operating which connects the location where the short dipoles are deployed with the nearby village of Lagada (see Figs. 4.2.3 and 1.4.1(b) of Ref. 22). Considering the value ΔV_{long} measured at this dipole (*cf.* $\Delta V_{long} \approx$ 20 mV, see the lowest panel of Fig. 1(b) of Ref. 24) we find that the ratio $\Delta V_{long}/\Delta V_{short}$ in the present case (*e.g.* $\Delta V_{short} \approx 1.5$ mV when $L_{short} = 100$ m, see the first line of Table 1 where $E_{short} = E = 15$ μV/m) differs significantly from the ones observed in the past before EQs coming from the area 'c' of the selectivity map. For example, compare the SES activity under discussion (announced in Ref. 24) with the one recorded on 6 April 1995 at ASS — depicted in Fig. 4.2.2 of Ref. 22 — with $\Delta V_{long} \approx 13$ mV and $\Delta V_{short} \approx 0.4$ mV that preceded the M_w5.3 EQ on 4 May 1995 at 40.7°N, 23.5°E (marked with the yellow

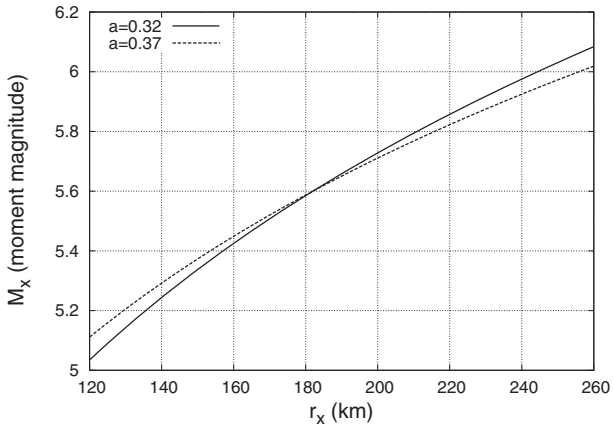

Fig. 3. The estimated magnitude M_x of the EQ related with the SES activity recorded on 13 July 2012 as a function of its focal distance r_x from ASS (the two curves correspond to the two limiting values of the constant a).

star in Fig. 2), *i.e.*, 40 km ESE of ASS. Thus, the area 'c' was excluded in the present case as a candidate area for the EQ epicenter.

We now turn to the magnitude of the EQ. This can be investigated on the basis of Eq. [1] by referring to an earlier SES recorded at ASS having an amplitude E_2 ($= 14\,\mu$V/m) comparable with that of the SES activity under discussion (see the second line of Table 1) and a focal distance r_2 ($= 195$ km). This was the case of the SES recorded on 25 April 1985 which preceded an $M_S(ATH)5.8$ EQ (Harvard reported M_w5.6) that occurred close to Volos city in central Greece on 30 April 1985, see the cyan star in Fig. 2. Using Eq. [1], we estimated the magnitude M_x ($= \log_{10}(r_x E_1/r_2 E_2)/a + M_2$) versus the focal distance r_x from ASS as shown in Fig. 3. We observe that for r_x in the range 120 to 260 km (*cf.* area 'c' was already excluded as mentioned) M_x varies between 5 to 6 magnitude units. The actual focal distance r_1 was 250 km leading to $M_x \approx 6.0$. The latter value compares favourably with the observed $5.8 M_w$ EQ if we also take into account a plausible estimation error.

4. Identifying the EQ occurrence time on the basis of natural time analysis

A procedure to identify the time window of an impending mainshock has been developed[13),19),21)] based on the hypothesis that the occurrence of a mainshock can be considered as a critical point (*e.g.* Ref. 25, see also Ref. 26 and references therein). As mentioned in Section 2, it has been observed that when the system enters the critical stage, the variance κ_1 calculated using a seismic catalogue approaches the value $\kappa_1 = 0.070$ provided that the calculation is started at the initiation time of SES. If major EQs are critical phenomena, this property should be observed in a wide spatial range due to the unavoidable development of long range correlations, *e.g.* see Ref. 20. Thus, once an SES activity has been recorded at a station we start studying the seismicity in the area to suffer a mainshock based on the selectivity map of the station. In this area, hereafter labelled A, we examine the small events (EQs) — with magnitudes greater or equal to a threshold M_{thres} — that occur after the initiation of the SES activity. Analyzing in natural time this subsequent seismicity as it evolves event by event in area A as well as in *all* the possible subareas of A (*cf.* practically we use only rectangular subareas delimited by the epicenters of small EQs as an approximation as shown in Fig. 4, see also Fig. 1 of Ref. 21) we can obtain a multitude of κ_1 values that enable the construction of the distribution of κ_1, labeled Prob(κ_1). When the critical stage is approached the condition $\kappa_1 = 0.070$ should exhibit spatial invariance leading to a maximum of Prob(κ_1) at $\kappa_1 \approx 0.070$. Moreover, the scale invariance associated with critical phenomena implies that the same picture is expected to hold if we also vary the magnitude threshold. Thus, the simultaneous observation of maxima of Prob(κ_1) at $\kappa_1 \approx 0.070$ for various magnitude thresholds can indicate that the critical stage has been approached and the mainshock is imminent. It was found[13),21)] that such a behavior usually occurs a few days to around one week *before* the mainshock, making the time window of prediction to the order of a week or less as already mentioned in Section 2.

Figure 2 depicts with red circles all the small EQs that occurred after the SES and before the M_w5.8 event within the area $N_{38.7}^{41.5} E_{21.9}^{25.7}$ (blue dashed rectangle) that surrounds the Assiros selectivity map. We observe that during this period a series of small EQs occurred close to Lamia city (LAM): these EQs cannot be related with SES at Assiros because they lie well outside the already known selectivity map (areas 'a', 'b', 'c') and if they were related to some SES, the corresponding SES should have been recorded according to our experience[13),22)] at the nearby LAM station and not at ASS. In order to exclude the majority of them from the calculation without missing events that occurred within the selectivity map of ASS, we moved the Western

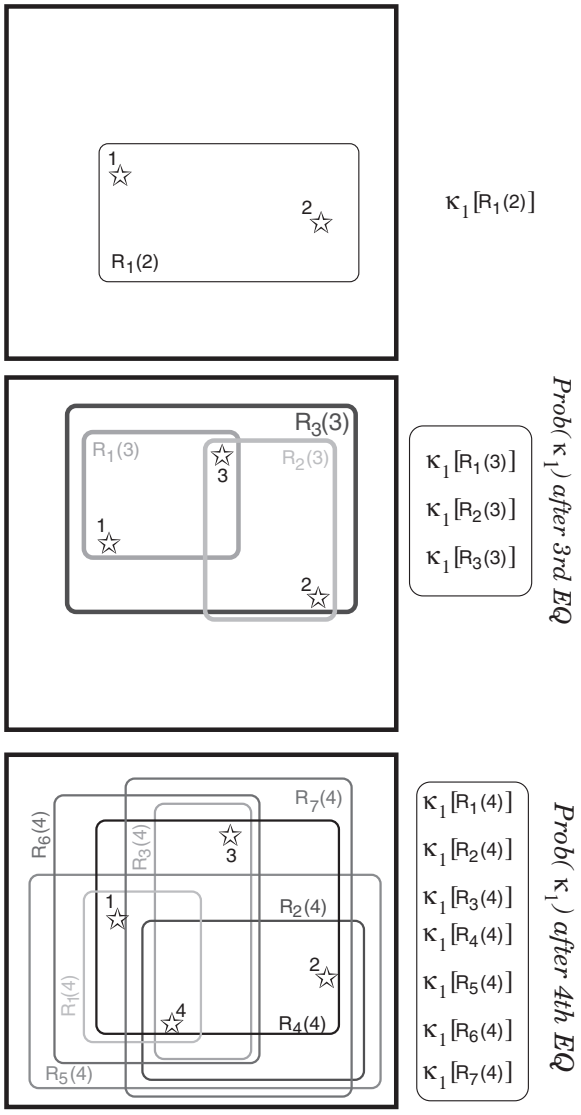

Fig. 4. The area A (in thick black rectangle) together with a series of 4 EQs (depicted with the open stars) that occurred inside this area in the sequence in which they are numbered. The three panels show the rectangular subareas $R_j(i)$ in each of which the seismicity is used for the calculation of κ_1 after the occurrence of the i-th EQ. Each rectangular subarea is defined so that it necessarily includes the last EQ, *i.e.*, the i-th EQ. For example, in the upper panel, which depicts the situation after the second EQ, only one such subarea, *i.e.*, $R_1(2)$, can be defined. In the middle panel, after the third EQ, three such subareas exist leading to 3, in general different, κ_1 values. In the lower panel, after the fourth EQ, seven rectangular subareas are used for the calculation of the κ_1 values. These values are used for the construction of the distribution Prob(κ_1) after the fourth EQ. This procedure is followed after the occurrence of each new small EQ within area A as discussed in the text. The assumption of the rectangular shape of the subareas simplifies their calculation — and hence the calculation of Prob(κ_1) — because each subarea is limited by the latitude and the longitude of the EQ epicenters and must also include the last EQ.

boundary by 0.6° to the East (as well the Eastern boundary 0.1° to the West so that it coincides with the Eastern boundary of the selectivity map) and applied the aforementioned procedure for the natural time analysis of seismicity assuming that area A is $N_{38.7}^{41.5}E_{22.5}^{25.6}$ (drawn with a green dotted rectangle in Fig. 2) which practically surrounds the ASS selectivity map excluding its Western part.

Here, in our analysis we used the local magnitudes (M_L) reported by the seismic catalogue of the Institute of Geodynamics of the National Observatory of Athens (www.gein.noa.gr). A major improvement of the seismological network of this Institute has been recently completed.[27)–31)]

Figure 5 shows that on 5 January 2013, upon the occurrence of the $M_L = 2.9$ event at 05:55 UT, Prob(κ_1) for $M_{thres} = 2.9$ maximized at $\kappa_1 \approx 0.070$. This behavior also exhibits magnitude threshold invariance since it holds for magnitude thresholds $M_{thres} = 2.9$, 2.8 and 2.7. As said, the fulfillment of the condition $\kappa_1 \approx 0.070$ signals that the system has approached the critical point and actually the M_w5.8 EQ occurred on 8 January 2013.

5. Construction of a new selectivity map for ASS

The fact that the epicenter of the 8 January 2013 EQ lies just outside the existing selectivity map of ASS prompted us to improve it (*cf.* it has been already suggested[13)] that areas 'a', 'b' and 'c' may be interconnected into a single large region but since no large EQs had occurred in the intermediate region no significant SES has been correlated to them so far). To this end, we depict in Fig. 2 with the red dashed-dotted curve the proposed new selectivity map of ASS — in which the natural time analysis of seismicity should be performed — and mark with blue plus symbols the small EQs that occurred inside it after the SES initiation and before the M_w5.8 EQ. If the proposal is correct, the exclusion of small EQs not related with the SES at Assiros (*e.g.* see the events that occurred in the South-Southeastern part of the original area $N_{38.7}^{41.5}E_{22.5}^{25.6}$) will lead to a more evident correlation between the EQs studied and hence the results of Fig. 5 should be improved. The results of this analysis for $M_{thres} = 3.0$ are shown in Fig. 6. We observe a clearly better shape of the peak at $\kappa_1 \approx 0.070$ upon the occurrence of the $M_L = 3.0$ EQ on 27 December 2012, which is the last one (for this magnitude threshold) before the M_w5.8 EQ. Moreover, the peak at $\kappa_1 \approx 0.070$ is also observed upon the occurrence of the aforementioned $M_L = 2.9$ event on 5 January 2013 at 05:55 UT

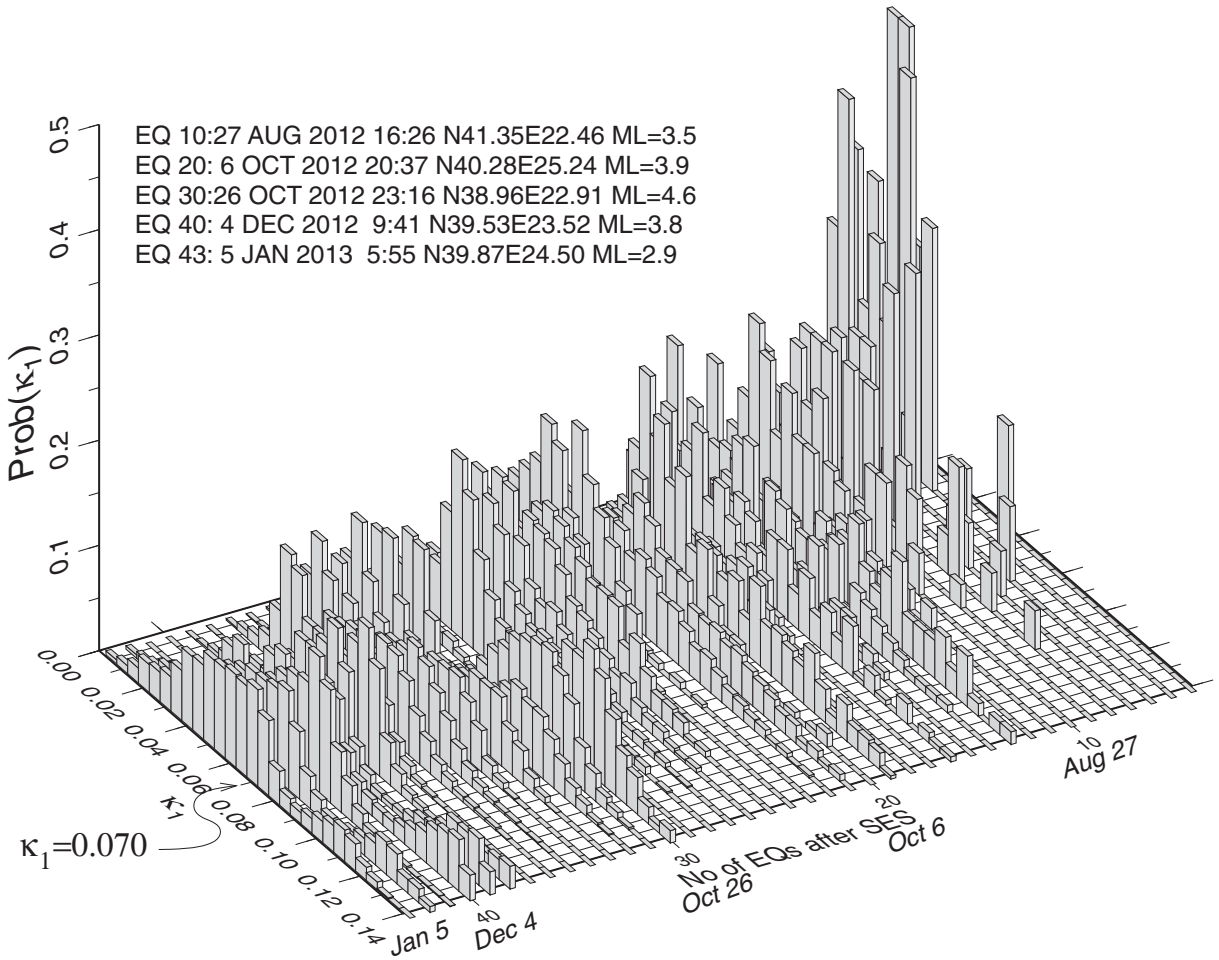

Fig. 5. Estimation of the occurrence time of the M_w5.8 EQ that occurred on 8 January 2013: The calculation is based on the natural time analysis of the EQs that occurred after the SES initiation until 5 January 2013 inside the region $N_{38.7}^{41.5}E_{22.5}^{25.6}$ (dotted green rectangle in Fig. 2). The figure depicts the histogram of Prob(κ_1) versus κ_1 after each such EQ for $M_{thres} = 2.9$. The occurrence time (UT) and magnitude for some of these EQs are written in the upper left part. The last event is the $M_L = 2.9$ EQ that occurred at 05:55 UT on 5 January 2013 which is shown with a green circle in Fig. 2.

Prob(κ_1) for $M_{thres} = 2.9$, 2.8 and 2.7. We note that both the $M_L = 3.0$ and the $M_L = 2.9$ EQs occurred very close in space with epicenters at 39.81°N, 24.45°E and 39.87°N, 24.50°E (*cf.* the latter epicenter is marked with a green circle in Fig. 2 and lies 92 km west of the epicenter of the M_w5.8 EQ on 8 January 2013).

6. Conclusions

By analyzing in natural time the seismicity that occurred inside a rectangular region surrounding the already known ASS selectivity map after the initiation of the SES activity recorded at ASS on 13 July 2012, we identified that the condition $\kappa_1 \approx 0.070$ was fullfilled on 5 January 2013 and hence a major EQ would be imminent. Actually on 8 January 2013 an $M_S(ATH) = 6.2$ ($M_w = 5.8$) EQ occurred close to the eastern edge of this rectangular region. Moreover, the properties of the SES activity allows the determination of the epicentral location and magnitude which are reasonably compatible with those of the M_w5.8 event. In short, all the parameters (epicenter, magnitude and time-window) of this EQ could be estimated on the basis of the SES properties together with natural time analysis. This strengthens the view that SES measurements are valuable for short-term EQ prediction. In addition, the present results indicate that the selectivity map of Assiros station should be augmented to include also the epicenter of the last EQ.

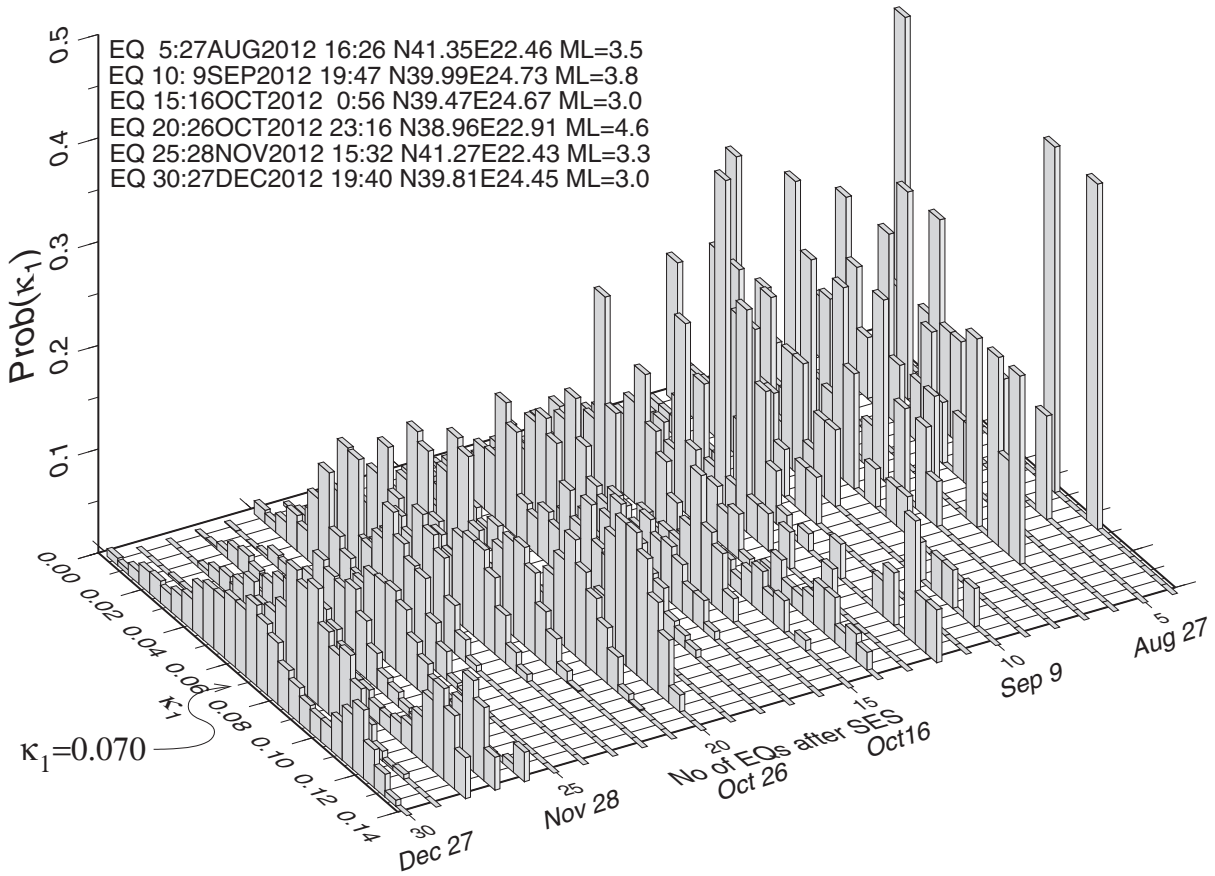

Fig. 6. The same as in Fig. 5, but by considering only the EQs — marked with blue plus symbols in Fig. 2 — that lie inside the proposed selectivity map of ASS. The figure depicts the histograms of Prob(κ_1) versus κ_1 for $M_{thres} = 3.0$.

Acknowledgements

The author would like to express his sincere thanks to Professor Seiya Uyeda, M.J.A., who carefully went through the present manuscript and made several useful and intuitive remarks.

References

1) Uyeda, S., Nagao, T. and Kamogawa, M. (2009) Short-term earthquake prediction: Current status of seismo-electromagnetics. Tectonophysics **470**, 205–213.
2) Hayakawa, M. (ed.) (2013) The Frontier of Earthquake Prediction Studies. Nihon-Senmontosho-Shuppan, Tokyo.
3) Hayakawa, M. (ed.) (2013) Earthquake Prediction Studies: Seismo Electromagnetics. Terrapub, Tokyo.
4) Varotsos, P. and Alexopoulos, K. (1984) Physical properties of the variations of the electric field of the earth preceding earthquakes, I. Tectonophysics **110**, 73–98.
5) Varotsos, P. and Alexopoulos, K. (1984) Physical properties of the variations of the electric field of the earth preceding earthquakes, II. Tectonophysics **110**, 99–125.
6) Varotsos, P. and Lazaridou, M. (1991) Latest aspects of earthquake prediction in Greece based on seismic electric signals. Tectonophysics **188**, 321–347.
7) Varotsos, P., Alexopoulos, K. and Lazaridou, M. (1993) Latest aspects of earthquake prediction in Greece based on seismic electric signals, II. Tectonophysics **224**, 1–37.
8) Uyeda, S. and Kamogawa, M. (2008) The prediction of two large earthquakes in Greece. Eos Trans. AGU **89**, 363.
9) Uyeda, S. and Kamogawa, M. (2010) Comment on 'The prediction of two large earthquakes in Greece'. Eos Trans. AGU **91**, 163.
10) Uyeda, S., Nagao, T., Orihara, Y., Yamaguchi, T. and Takahashi, I. (2000) Geoelectric potential changes: Possible precursors to earthquakes in Japan. Proc. Natl. Acad. Sci. U.S.A. **97**, 4561–4566.
11) Uyeda, S., Hayakawa, M., Nagao, T., Molchanov, O., Hattori, K., Orihara, Y., Gotoh, K., Akinaga, Y. and Tanaka, H. (2002) Electric and magnetic phenomena observed before the volcano-seismic

activity in 2000 in the Izu Island region, Japan. Proc. Natl. Acad. Sci. U.S.A. **99**, 7352–7355.
12) Orihara, Y., Kamogawa, M., Nagao, T. and Uyeda, S. (2012) Preseismic anomalous telluric current signals observed in Kozu-shima Island, Japan. Proc. Natl. Acad. Sci. U.S.A. **109**, 19125–19128.
13) Varotsos, P.A., Sarlis, N.V. and Skordas, E.S. (2011) Natural Time Analysis: The new view of time. Precursory Seismic Electric Signals, Earthquakes and other Complex Time-Series. Springer-Verlag, Berlin, Heidelberg.
14) Lazaridou-Varotsos, M.S. (2013) Earthquake Prediction by Seismic Electric Signals: The success of the VAN method over thirty years. Springer-Verlag, Berlin, Heidelberg.
15) Varotsos, P., Sarlis, N., Lazaridou, M. and Kapiris, P. (1998) Transmission of stress induced electric signals in dielectric media. J. Appl. Phys. **83**, 60–70.
16) Sarlis, N., Lazaridou, M., Kapiris, P. and Varotsos, P. (1999) Numerical model of the selectivity effect and ΔV/L criterion. Geophys. Res. Lett. **26**, 3245–3248.
17) Surkov, V.V., Uyeda, S., Tanaka, H. and Hayakawa, M. (2002) Fractal properties of medium and seismoelectric phenomena. J. Geodyn. **33**, 477–487.
18) Varotsos, P.A., Sarlis, N.V. and Skordas, E.S. (2002) Long-range correlations in the electric signals that precede rupture. Phys. Rev. E Stat. Nonlin. Soft Matter Phys. **66**, 011902.
19) Varotsos, P.A., Sarlis, N.V., Tanaka, H.K. and Skordas, E.S. (2005) Similarity of fluctuations in correlated systems: The case of seismicity. Phys. Rev. E Stat. Nonlin. Soft Matter Phys. **72**, 041103.
20) Varotsos, P., Sarlis, N.V., Skordas, E.S., Uyeda, S. and Kamogawa, M. (2011) Natural time analysis of critical phenomena. Proc. Natl. Acad. Sci. U.S.A. **108**, 11361–11364.
21) Sarlis, N.V., Skordas, E.S., Lazaridou, M.S. and Varotsos, P.A. (2008) Investigation of seismicity after the initiation of a seismic electric signal activity until the main shock. Proc. Jpn. Acad., Ser. B **84**, 331–343.
22) Varotsos, P. (2005) The Physics of Seismic Electric Signals. Terrapub, Tokyo.
23) Kondo, S., Uyeda, S. and Nagao, T. (2002) The selectivity of Ioannina VAN station. J. Geodyn. **33**, 433–461.
24) Varotsos, P.A., Sarlis, N.V. and Skordas, E.S. (2012) Order parameter fluctuations in natural time and b-value variation before large earthquakes. Nat. Hazards Earth Syst. Sci. **12**, 3473–3481.
25) Klein, W., Gould, H., Gulbahce, N., Rundle, J.B. and Tiampo, K. (2007) Structure of fluctuations near mean-field critical points and spinodals and its implication for physical processes. Phys. Rev. E Stat. Nonlin. Soft Matter Phys. **75**, 031114.
26) Sornette, D. (2004) Critical Phenomena in Natural Science. 2nd ed. Springer-Verlag, Berlin Heidelberg.
27) Chouliaras, G. (2009) Investigating the earthquake catalog of the National Observatory of Athens. Nat. Hazards Earth Syst. Sci. **9**, 905–912.
28) Melis, N.S. and Konstantinou, K.I. (2006) Real-time seismic monitoring in the Greek region: An example from the 17 October 2005 East Aegean Sea earthquake sequence. Seismol. Res. Lett. **77**, 364–370.
29) Konstantinou, K.I., Melis, N.S. and Boukouras, K. (2010) Routine regional moment tensor inversion for earthquakes in the Greek region: The National Observatory of Athens (NOA) database (2001–2006). Seismol. Res. Lett. **81**, 750–760.
30) Evangelidis, C.P. and Melis, N.S. (2012) Ambient noise levels in Greece as recorded at the Hellenic Unified Seismic Network. Bull. Seismol. Soc. Am. **102**, 2507–2517.
31) Chouliaras, G., Melis, N.S., Drakatos, G. and Makropoulos, K. (2013) Operational network improvements and increased reporting in the NOA (Greece) seismicity catalog. Adv. Geosci. **36**, 7–9.

(Received Sep. 21, 2013; accepted Oct. 3, 2013)